

Study on divertor plasma behavior through sweeping strike point in new lower divertor on EAST

Yu-Qiang Tao(陶余强), Guo-Sheng Xu(徐国盛), Ling-Yi Meng(孟令义), Rui-Rong Liang(梁瑞荣), Lin Yu(余林), Xiang Liu(刘祥), Ning Yan(颜宁), Qing-Quan Yang(杨清泉), Xin Lin(林新), and Liang Wang(王亮)

Citation: Chin. Phys. B, 2022, 31 (**6**): 065204. DOI: 10.1088/1674-1056/ac4a65
Journal homepage: http://cpb.iphy.ac.cn; http://iopscience.iop.org/cpb

What follows is a list of articles you may be interested in

Observation of trapped and passing runaway electrons by infrared camera in the EAST tokamak

Yong-Kuan Zhang(张永宽), Rui-Jie Zhou(周瑞杰), Li-Qun Hu(胡立群), Mei-Wen Chen(陈美文), Yan Chao(晁燕), Jia-Yuan Zhang(张家源), and Pan Li(李磐)
Chin. Phys. B, 2021, 30 (**5**): 055206. DOI: 10.1088/1674-1056/abd758

Analysis of asymmetry of the D_α emission spectra under the Zeeman effect in boundary region for D-D experiment on EAST tokamak

Wei Gao(高伟), Juan Huang(黄娟), Jianxun Su(宿建勋), Jing Fu(付静), Yingjie Chen(陈颖杰), Wei Gao(高伟), Zhenwei Wu(吴振伟), and EAST Team
Chin. Phys. B, 2021, 30 (**2**): 025201. DOI: 10.1088/1674-1056/abc162

Measurement of molybdenum ion density for L-mode and H-mode plasma discharges in the EAST tokamak

Yongcai Shen(沈永才), Hongming Zhang(张洪明), Bo Lyu(吕波), Yingying Li(李颖颖), Jia Fu(符佳), Fudi Wang(王福地), Qing Zang(臧庆), Baonian Wan(万宝年), Pan Pan(潘盼), Minyou Ye(叶民友)
Chin. Phys. B, 2020, 29 (**6**): 065206. DOI: 10.1088/1674-1056/ab8456

Plasma shape optimization for EAST tokamak using orthogonal method

Yuan-Yang Chen(陈远洋), Xiao-Hua Bao(鲍晓华), Peng Fu(傅鹏), Ge Gao(高格)
Chin. Phys. B, 2019, 28 (**1**): 015201. DOI: 10.1088/1674-1056/28/1/015201

Synchrotron radiation intensity and energy of runaway electrons in EAST tokamak

Y K Zhang(张永宽), R J Zhou(周瑞杰), L Q Hu(胡立群), M W Chen(陈美文), Y Chao(晁燕), EAST team
Chin. Phys. B, 2018, 27 (**5**): 055206. DOI: 10.1088/1674-1056/27/5/055206

Study on divertor plasma behavior through sweeping strike point in new lower divertor on EAST

Yu-Qiang Tao(陶余强)[1,2], Guo-Sheng Xu(徐国盛)[1,†], Ling-Yi Meng(孟令义)[1,2], Rui-Rong Liang(梁瑞荣)[1,2], Lin Yu(余林)[1,2], Xiang Liu(刘祥)[1], Ning Yan(颜宁)[1], Qing-Quan Yang(杨清泉)[1], Xin Lin(林新)[1], and Liang Wang(王亮)[1,3,‡]

[1] *Institute of Plasma Physics, Hefei Institutes of Physical Science, Chinese Academy of Sciences, Hefei* 230031, *China*
[2] *University of Science and Technology of China, Hefei* 230026, *China*
[3] *Institute of Energy, Hefei Comprehensive National Science Center, Hefei* 230031, *China*

(Received 28 October 2021; revised manuscript received 7 January 2022; accepted manuscript online 12 January 2022)

A series of L-mode discharges have been conducted in the new 'corner slot' divertor on the Experimental Advanced Superconducting Tokamak (EAST) to study the divertor plasma behavior through sweeping strike point. The plasma control system controls the strike point sweeping from the horizontal target to the vertical target through poloidal field coils, with keeping the main plasma stability. The surface temperature of the divertor target cools down as the strike point moves away, indicating that sweeping strike point mitigates the heat load. To avoid the negative effect of probe tip damage, a method based on sweeping strike point is used to get the normalized profile and study the decay length of particle and heat flux on the divertor target λ_{js}, λ_q. In the discharges with high radio-frequency (RF) heating power, electron temperature T_e is lower and λ_{js} is larger when the strike point locates on the horizontal target compared to the vertical target, probably due to the corner effect. In the Ohmic discharges, λ_{js}, λ_q are much larger compared to the discharges with high RF heating power, which may be attributed to lower edge T_e.

Keywords: EAST tokamak, divertor plasma, sweeping strike point, decay length

PACS: 52.55.Ez, 52.55.Rk, 52.40.–w **DOI:** 10.1088/1674-1056/ac4a65

1. Introduction

In tokamaks, heat and particles exhausted from the hot magnetically confined plasma, stream along open magnetic field lines and mainly localize over lengths much shorter than the size of divertor target plates. For future reactors, the unmitigated heat load on divertor target is more than one order larger than the engineering safety limit, ~ 10 MW/m^2, which is a severe challenge.[1] Several solutions are proposed to mitigate the high heat load: distribute heat fluxes through manipulating divertor poloidal magnetic configurations, such as snowflake divertor[2] and super-X divertor;[3] facilitate detachment through trapping neutrals and impurities in a highly closed divertor, such as SAS divertor on DIII-D[4] and the new 'corner slot' divertor on EAST.[1] There is another simple and robust method, sweeping strike point, to spread the heat load over a large surface area. Sweeping strike point experiments have been successfully conducted in JET experiments, and this method may be adopted in the future campaign with 40 MW of source auxiliary heating power.[5] Similar concept, the fish tail divertor (FTD), has been proposed and experimentally performed on EAST,[6,7] which needs an additional alternating magnetic field coil behind the divertor. Some studies have so far found that sweeping appears to be compatible with implementation and use on DEMO.[8]

In this year, EAST superconducting tokamak has replaced the old lower graphite divertor with tungsten divertor to increase the power handling capacity to ~ 10 MW/m^2. The most attractive characteristic of this new divertor is the 'corner slot', *i.e.*, a closed right-angle corner consisted by the horizontal target and vertical target. This special structure can bring the 'corner effect', *i.e.*, when the outer strike point locates on the horizontal target plate near the corner, the horizontal target plate reflects impinging particles mostly towards the scrape-off layer (SOL), where the particles are confined by the vertical target plate and trapped in the closed corner, thus high neutral pressure is achieved near the corner. The corner effect has been studied by SOLPS-ITER simulation.[1]

In this paper, the divertor plasma behavior will be studied through sweeping strike point in the new lower divertor on EAST. Owning to the powerful control ability of poloidal field coils, the plasma control system (PCS) adjusts the location of primary X-point flexibly and controls the lower outer strike point sweeping from the horizontal target to the vertical target. Surface temperature will be monitored by infrared (IR) thermography to demonstrate that sweeping strike point can mitigate the heat load on divertor target. Plasma behavior, such as divertor particle flux and heat flux, will be diagnosed by divertor Langmuir probe array. To avoid the effect of probe

†Corresponding author. E-mail: gsxu@ipp.ac.cn
‡Corresponding author. E-mail: lwang@ipp.ac.cn

© 2022 Chinese Physical Society and IOP Publishing Ltd

tip damage, a method based on sweeping strike point is applied to get the normalized distributions on the divertor target, similar to the technique in the work.[9] And the decay lengths of divertor particle flux and heat flux, λ_{js}, λ_q, will be discussed and compared with previous work.[10–12]

This paper is organized as follows: Section 2 describes the experimental setup and introduces the relevant diagnostics; Section 3 presents the experimental results and discussion. Summary is given in Section 4.

2. Experimental setup and main diagnostics

A series of sweeping strike point experiments have been conducted in EAST low confinement mode (L-mode) discharges with high RF heating power. The discharges are operated in lower single null (LSN) or double null (DN) divertor configuration. The central magnetic field is $B_t = 2.4$ T with the ion $B \times \nabla B$ drift direction into upper divertor. Figure 1(a) shows the configuration of one typical LSN shot #98332, calculated from EFIT magnetic reconstruction. The PCS controls the X-point moving towards low field side from $R_x \sim 159$ cm (3 s) to $R_x \sim 166$ cm (8 s), where R_x is the major radius of the lower X-point. Consequently, the lower outer strike point sweeps from the horizontal target to the vertical target, as seen in Fig. 1(c). The distance between strike point and the corner is nearly linear with time, when the strike point locates on the horizontal target or vertical target, as shown in Fig. 1(b).

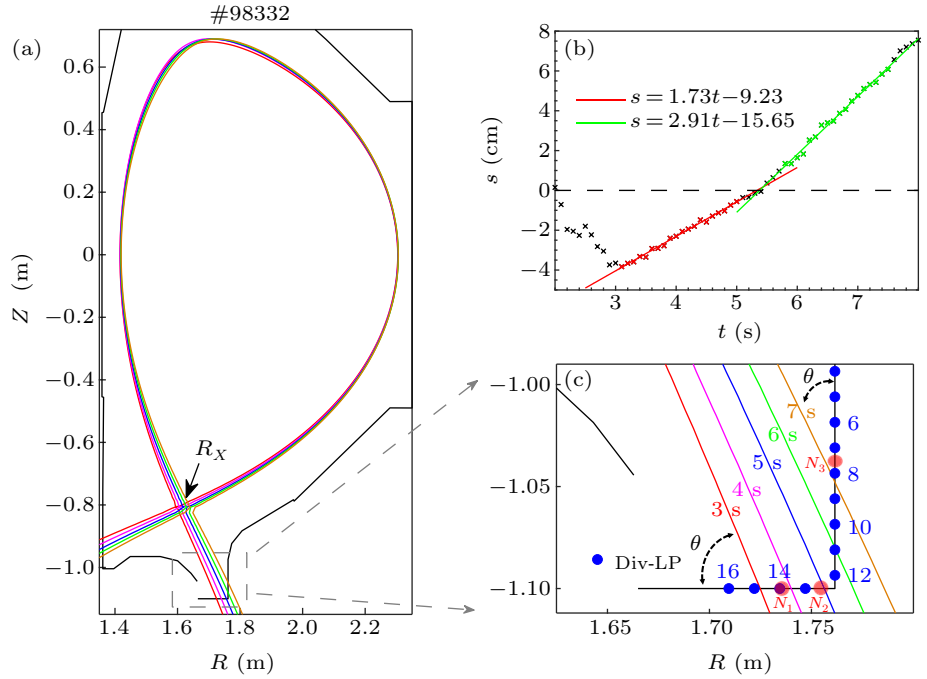


Fig. 1. In shot #98332, (a) the magnetic configurations at different times; (b) the distance (s) between lower outer strike point and the corner *versus* time (t) with linear fit on the horizontal target ($s < 0$) and vertical target ($s > 0$); (c) detail view in the lower outer divertor region with the distribution of divertor Langmuir probe array (Div-LP), the intersection angle θ ($\theta < 90°$) between the poloidal magnetic field and the target plate, and the pixel location N_1, N_2, N_3 (red ellipses).

During these discharges, the plasma current is $I_p = 500$ kA in Fig. 2(a). The source auxiliary heating power is $P_{total} = 3.2$ MW including 0.7 MW from 2.45G low hybrid wave (LHW), 2 MW from 4.6G LHW, and 0.5 MW from electron cyclotron resonance heating (ECRH), as shown in Fig. 2(b). The displacement of primary X-point unavoidably brings the change of the main plasma shape. The main change is the lower triangularity, which varies up to $\sim 20\%$. However, the elongation only varies below 2% and the edge safety factor varies below 0.5%. It is worthy to mention that the magnetic geometry on the outer mid-plane differs slightly, as shown in Fig. 1(a), where the auxiliary heating system locates. The main plasma keeps stable as the strike point sweeps. The central-line averaged electron density is $n_{el} \sim 2 \times 10^{19}$ m^{-3}, which has slight increase ($\leq 10\%$) in Fig. 2(c). And the plasma stored energy is ~ 110 kJ, as seen in Fig. 2(d). Besides, two Ohmic discharges are also conducted in DN configuration with the similar parameters (shots #98895 and #98896).

Main diagnostics used in this work include the infrared (IR) thermography[13] and the divertor Langmuir probe array.[14,15] Two integrated infrared and visible tangential wide-angle viewing systems have been mounted in EAST to provide real-time, simultaneously visible and infrared imaging of the vacuum vessel, including the lower divertor region. The principle of infrared thermography to monitor the surface temperature of objects is based on black-body radiation law with considering the impact of the radiometric factors on the measurement of the camera.[13] Though the heat flux code of

the infrared thermography is under programming, the surface temperature roughly reveals the heat load on divertor target. EAST has installed two divertor Langmuir probe array[14,15] in port D and port P with the same poloidal distribution, as shown in Fig. 1(c). Each array has 16 channels: four localize on the horizontal target (#13–#16), and the others localize on the vertical target (#1–#12). The probe array is based on triple probe and used to measure the positive biased potential V_p, the ion saturation current I_s and the floating potential V_f. Based on $T_e = (V_p - V_f)/\ln 2$ and $J_s = I_s/A_{pr}$, electron temperature T_e and particle flux $\Gamma_{ion} = J_s/e$ are obtained, where e is elementary charge and A_{pr} is the effective area of a probe tip. The parallel heat flux $q_{\parallel}$ and electron density n_e are further obtained by $q_{\parallel} = \gamma_{sh}\Gamma_{ion}T_e$, $n_e = I_s/[eA_{pr}(2T_e/m_i)^{1/2}]$, where $\gamma_{sh} \approx 7$ is the electron sheath heat transmission coefficient, m_i is the ion mass.

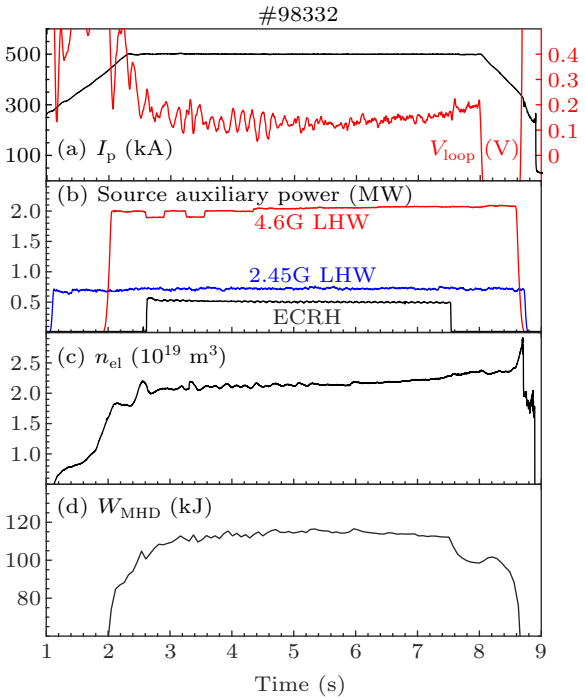


Fig. 2. (a) Plasma current I_p (black) and loop voltage V_{loop} (red); (b) the source power P_{source} of auxiliary heating system; (c) the central-averaged averaged electron density n_{el}; (d) the plasma stored energy W_{MHD}.

3. Experimental results and discussion

3.1. Surface temperature

When the strike point sweeps, the heat flux also moves with strike point and the heat load on divertor target is mitigated through large surfaces. In the shot #98332 with $P_{total} = 3.2$ MW, the bright ring moves with strike point from the horizontal target to the vertical target, as shown in Fig. 3. And the ring is brightest when the strike point is near the corner, and darkest when the strike point is on the vertical target.

A pixel path is chosen, as shown in the Fig. 3(b), to get the time trace of surface temperature, as seen in Fig. 4. Limited to spatial resolution and mechanical vibration, it is hard to obtain the exact location of each pixel. Here we give numbers to the pixels, and $N_{pixel} < 0$ is on the horizontal target, $N_{pixel} > 0$ is on the vertical target, and $N_{pixel} = 0$ is around the corner. From 3 s–8 s, the peak surface temperature obviously moves with strike point. After the strike point moves away, the local surface temperature decreases, which demonstrate that sweeping strike point mitigates the heat load on divertor target.

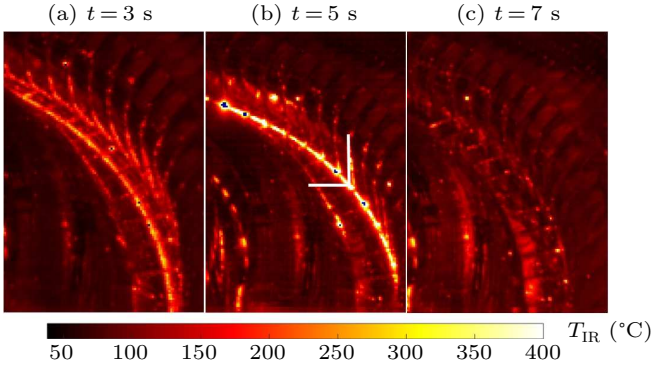


Fig. 3. Three IR camera frames with the colorbar of surface temperature T_{IR} at 3, 5, and 7 s in the lower outer region of shot #98332. The white path in panel (b) is used to get the time trace of surface temperature.

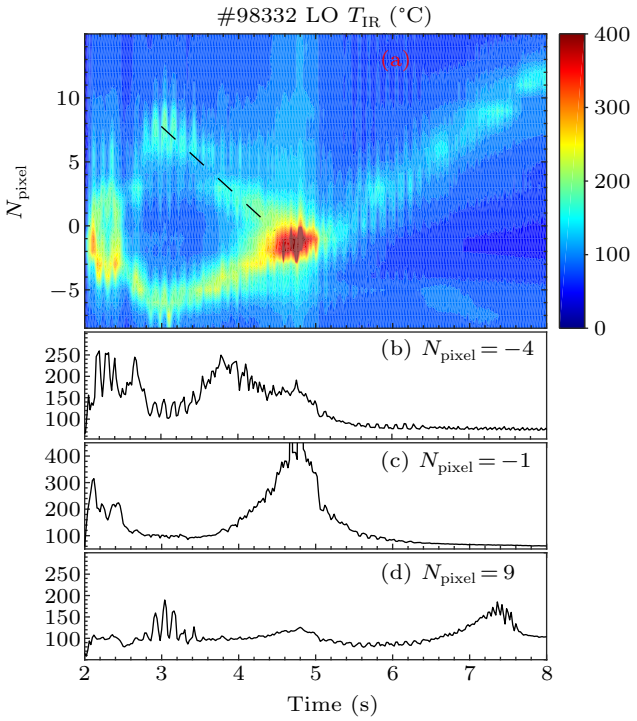


Fig. 4. (a) Time traces of surface temperature T_{IR} (°C) for the pixel path shown in Fig. 3(b) with the reflective ring (black dashed line); (c)–(d) surface temperature evolution of the pixel $N_{pixel} = -4, -1, 9$ with the approximate location N_1, N_2, N_3 respectively in Fig. 1(c).

The peak surface temperature differs largely for different regions. The peak surface of $N_{pixel} = -4$ on the horizontal target (away from corner) is ~ 240 °C, $\sim 40\%$ larger compared to $N_{pixel} = 9$ on the vertical target, as shown in Figs. 4(b) and 4(d). This difference is mainly attributed to the intersection angle θ ($\theta < 90°$) between the poloidal magnetic field and the

target plate, as shown in Fig. 1(c). Without significant energy dissipation, the parallel heat flux $q_{\parallel}$ should have slight change in the divertor region as the strike point sweeps. And the heat load q_t on the target plate is expressed as $q_t \approx q_{\parallel} \sin\varphi \sin\theta$, where the intersection angle φ between the magnetic field and the toroidal direction is almost the same as the strike point sweeps. The intersection angle θ is larger when the strike point locates on the horizontal target compared to the vertical target, as shown in Fig. 1(c). Thus, the heat load q_t on the horizontal target is larger than that on the vertical target.

Another remarkable phenomenon is that as the strike point moves near the corner, the surface temperature becomes very high, as shown in Fig. 4(a). The maximum surface temperature even exceeds 400 °C, as seen in Fig. 4(c). There are several possibilities for this phenomenon. (I) The distance between the surface and the water-cooling copper tubes near the corner is larger compared to other locations on the target plate, as seen in Fig. 6 of the article,[1] which leads to relatively weaker cooling capacity. (II) The reflection of light and energetic neutral particle by smooth tungsten surface becomes important as the strike point moves near the corner, which leads to heat accumulation. One evidence for (II) is that the reflective ring is observed in the Fig. 4(a).

3.2. The method to get normalized distributions of particle and heat flux on the divertor target

As the strike point sweeps, the plasma behavior can be diagnosed by divertor Langmuir probe array. However, the measured absolute values of electron density, particle and heat flux are affected by the serious ablation of graphite probe tips, especially during long-pulse operation or unmitigated disruptions.[14] In this paper, a method to overcome this drawback is applied to get the normalized distributions of particle and heat flux on the divertor target and study the decay lengths λ_{js}, λ_q, similar to the technique in the work.[9] As shown in Fig. 1(b), the movement of strike point on the horizontal target or vertical target is almost under the constant velocity, thus the time signal can be transferred to relative location information. The moment of peak T_e is transferred as the separatrix location.

With the assumption that the distribution on the divertor target changes slowly as the strike point sweeps, each probe can obtain the whole normalized distribution information of particle flux and heat flux. This assumption is checked through comparing the distributions provided by different probes. As shown in Fig. 5(a), probes #15, #14, and #13 on the horizontal target get the similar distributions of particle flux on the target, which verifies the assumption. The distributions on the vertical target also support the statement, as shown in Fig. 5(b).

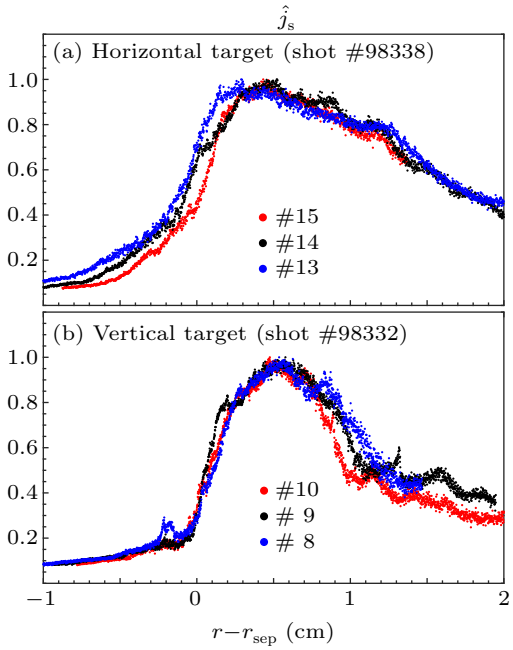


Fig. 5. Distributions of normalized particle flux on (a) the horizontal target and (b) vertical target. The former is diagnosed by probes #15, #14, and #13 in DN shot #98338; the latter is diagnosed by probes #10, #9, and #8 in LSN shot #98332.

3.3. Divertor plasma behavior with high RF heating power

In the discharges with high RF heating power, the plasma behaviors differ largely when the strike point locates on the horizontal target or vertical target. The plasma distributions on the divertor target in shot #98332 with $P_{total} = 3.2$ MW are shown in Fig. 6. To study λ_{js}, λ_q, a widespread fitting function[16,17] is used

$$y(x) = y_0 \exp\left[\left(\frac{S}{2\lambda}\right)^2 - \frac{x-x_0}{\lambda}\right] \times \mathrm{erfc}\left(\frac{S}{2\lambda} - \frac{x-x_0}{S}\right) + y_{BG},$$

where erfc is the Gauss error function, x_0 and y_{BG} are the separatrix location and background flux, S is introduced for the radial diffusion. The decay length λ is mapped to the outer midplane (OMP) to avoid the influence of connection length difference. As shown in Fig. 6(a), $\lambda_{js} = 5.6$ mm on the horizontal target is about twice as that on the vertical target (~ 2.7 mm). This difference may be due to the corner effect. When the strike point locates on the horizontal target, the target plate reflects impinging particles mostly towards the SOL. As a result, high neutral pressure is achieved near the corner, which significantly reduces local T_e in Fig. 6(b) and promote n_e in Fig. 6(d). λ_q on the horizontal target is also larger compared to the vertical target, as seen in Fig. 6(c).

We calculate λ_{js}, λ_q in several similar discharges with $P_{total} = 3.2$ MW, including shots #98313, #98332 in LSN configuration and shot #98338 in DN configuration. It is worthy to mention that the results of probes #12 and #11 are not included due to the following reason: both probes are close to

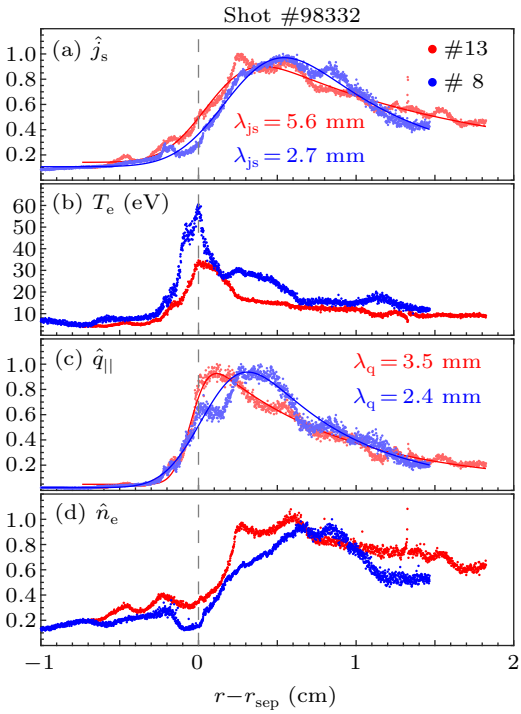


Fig. 6. In shot #98332, (a) the normalized particle flux $\hat{j}_s$, (b) the electron temperature T_e, (c) the normalized parallel heat flux $\hat{q}_{||}$, (d) the normalized electron density $\hat{n}_e$. The red is diagnosed by probing #13 on the horizontal target, and the blue is diagnosed by probe #8 on the vertical target. The solid lines in panels (a) and (c) are the fitting results with the decay length on the outer mid-plane.

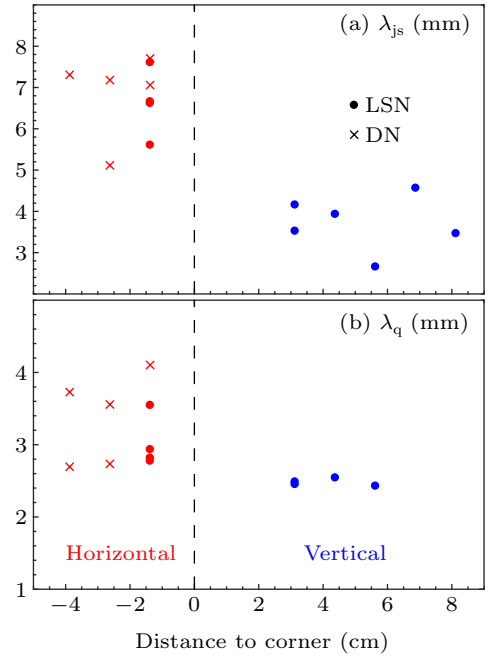


Fig. 7. Decay length of (a) divertor particle flux and (b) heat flux. The X-coordinate is the distance between the corresponding probe and the corner, and the negative is the horizontal target region and the positive is the vertical target region.

corner on the vertical target as seen in Fig. 1(c), as a result, the obtained distributions have the mixed information in which the SOL side are partly with strike point on the horizontal target, while the rest are with strike point on the vertical target. As shown in Fig. 7(a), λ_{js} on the horizontal target is nearly twice as that on the vertical target. λ_q on the horizontal target is also larger compared to the vertical target, as seen in Fig. 7(b). The weak corner effect on heat flux is probably due to low electron density or lack of energy dissipation, which still needs more research.

It is worthy to mention that the DN configuration does not narrow the decay length compared to LSN configuration, as seen in Fig. 7, consistent with previous work.[10] Besides, for the vertical target, $\lambda_{js}/\lambda_q \approx 1.3$, which shows that the divertor heat flux is mainly dominated by the divertor particle flux.[10,11] However, the ratio is much larger for the horizontal target, *i.e.* ~ 2, which may be due to the corner effect.

3.4. Divertor plasma behavior in the Ohmic discharges

The Ohmic discharges are also conducted with strike point sweeping, *i.e.*, shots #98895 and #98896. In the two shots, $n_{el} \approx 2 \times 10^{19}$ m^{-3} and $I_p = 500$ kA, which are similar with the shots mentioned above. Typical divertor plasma distributions are shown in Fig. 8. With $T_{e,peak} \sim 12$ eV, the heat flux distribution on the target is mainly dominated by the particle flux. $\lambda_{js} = 11.4$ mm and $\lambda_q = 10.3$ mm are obtained, which are significantly larger compared to the discharges with high RF heating power.

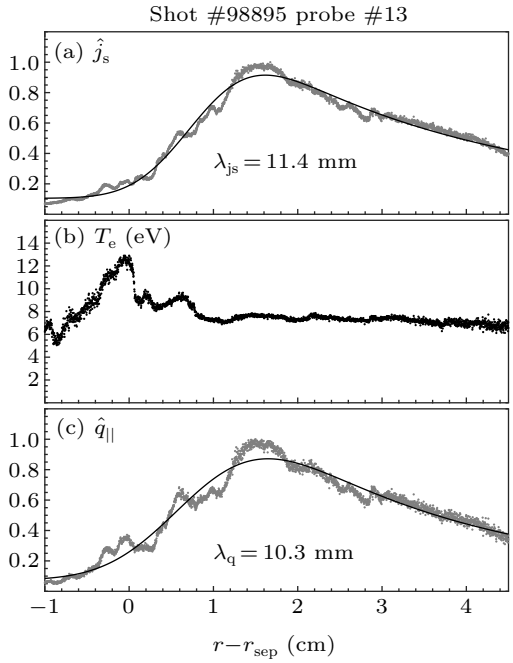


Fig. 8. In shot #98895, (a) the normalized particle flux $\hat{j}_s$, (b) the electron temperature T_e, (c) the normalized parallel heat flux provided by probe #13. The solid lines in panels (a) and (c) are the fitting results with the decay length on the outer mid-plane.

In these Ohmic discharges, the corner effect becomes weak. λ_{js} on the horizontal and vertical target is obtained, as shown in Fig. 9. And there is no clear difference between the horizontal target and vertical target, which implies that the corner effect is weak. The T_e measurement is poor in these two shots, and only few probes can provide the heat flux distributions, which are almost the same as Fig. 8(c).

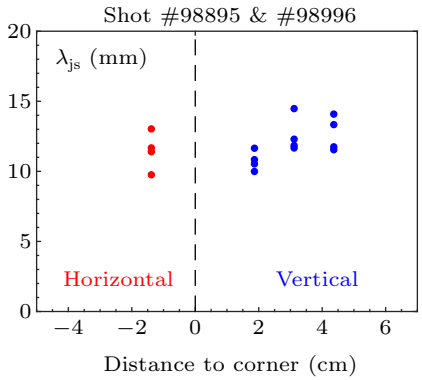


Fig. 9. Decay length of divertor particle flux λ_{js} in the Ohmic discharges. The X-coordinate is the same as Fig. 7.

3.5. Discussion on the decay length

The λ_{js}, λ_q in the Ohmic discharges are consistent with previous results.[10,11] However, they are much shorter in the discharges with high RF heating power. The difference may be due to the influence of the edge T_e. In ASDEX-Upgrade L-mode plasmas, λ_q scaling yields $\lambda_q \propto T_{e,edge}^{-0.93}$, where $T_{e,edge}$ is the edge electron temperature inside the separatrix.[18] Simulation work based on EAST L-mode discharges also shows that the SOL power width is influenced by the edge electron temperature through both parallel and radial heat transport, and λ_q scaling yields $\lambda_q \propto T_{e,LCFS}^{-1.03}$, where $T_{e,LCFS}$ is the electron temperature at the last closed flux surface (LCFS).[12] Unfortunately, $T_{e,LCFS}$ is not measured in EAST experiments yet. In the experiments with $P_{total} = 3.2$ MW, $n_{el} \approx 2 \times 10^{19}$ m^{-3}, $T_{e,LCFS}$ should be much higher than that in the Ohmic discharges or the shots with only 1-MW source auxiliary power.[10,11] As a result, higher $T_{e,LCFS}$ may shorten λ_{js}, λ_q.

4. Summary

In this paper, divertor plasma behavior through sweeping strike point recently conducted on EAST, which has upgraded the lower divertor with closed corner structure. As the strike point sweeps from the horizontal target and vertical target, the peak surface temperature of the divertor target measured by IR camera moves with strike point. And the local surface temperature successfully cools down as the strike point moves away, which indicate that the heat load is mitigated by sweeping strike point.

To study the behavior of particle flux and heat flux on the divertor target, a method based on sweeping strike point is used to avoid the effect of probe tip damage. λ_{js} on the horizontal target is almost twice as that on the vertical target, and T_e is also lower for the horizontal target. These differences may be due to the corner effect, which is one of the design thoughts of the new divertor with closed corner. In the Ohmic discharges, the corner effect seems weak and λ_{js}, λ_q are much larger than the discharges with high RF heating power. The underlying mechanism may be that higher edge T_e can narrow the λ_{js}, λ_q, consistent with the simulation results.[12]

Acknowledgments

The authors would like to acknowledge collaboration of the EAST team. Project supported by the National Key Research and Development Program of China (Grant No. 2017YFE0301300), the National Natural Science Foundation of China (Grant Nos. 12005257, 12005004, 11905143, and 11922513), the Fund from the Institute of Energy, Hefei Comprehensive National Science Center (Grant No. GXXT-2020-004), the CASHIPS Director's Fund (Grant Nos. BJPY2019A01 and YZJJ2020QN13), the Special Research Assistant Funding of CAS and China Postdoctoral Science Foundation (Grant No. 2020M671913), and Anhui Provincial Natural Science Foundation (Grant No. 2008085QA38).

References

[1] Xu G S, Wang L, Yao D M, Jia G Z, Sang C F, Liu X J, Chen Y P, Si H, Yang Z S, Guo H Y, *et al.* 2021 *Nucl. Fusion* **61** 126070
[2] Ryutov D D and Soukhanovskii V A 2015 *Phys. Plasmas* **22** 110901
[3] Valanju P M, Kotschenreuther M and Mahajan S M 2009 *Phys. Plasmas* **16** 056110
[4] Guo H Y, Wang H Q, Watkins J G, Casali L, Covele B, Moser A L, Osborne T, Samuell C M, Shafer M W and Stangeby P C 2019 *Nucl. Fusion* **59** 086054
[5] Silburn S A, Matthews G F, Challis C D, Frigione D, Graves J P, Mantsinen M J, Belonohy E, Hobirk J, Iglesias D and Keeling D L 2017 *Phys. Scr.* **2017** 014040
[6] Zhang X D *et al. Fishtail divertor: a new divertor concept on east for active control of heat load on divertor plate*, 2016 26th IAEA Fusion Energy Conference, 17–22 Kyoto, Japan
[7] Zhang Y *et al. Development of Fishtail Divertor for active control of heat load on EAST tokamak*, 2021 24th International Conference on Plasma–Surface Interaction in Controlled Fusion Devices, 24–29, Jeju, Korea
[8] Maviglia F, Federici G, Strohmayer G, Wenninger R, Bachmann C, Albanese R, Ambrosino R, Li M, Loschiavo V P, You J H and Zani L 2016 *Fusion Eng. Des.* **109** 1067
[9] Jaervinen A E, Allen S L, Eldon D, Fenstermacher M E, Groth M, Hill D N, Leonard A W, Mclean A G, Porter G D, Rognlien T D, Samuell C M and Wang H Q 2018 *Phys. Rev. Lett.* **121** 075001
[10] Liu J B, Guo H Y, Wang L, Xu G S, Wang H Q, Liu S C, Feng W, Xu J C, Deng G Z, Yang Q Q and Ling B L 2015 *Fusion Eng. Des.* **100** 301
[11] Wang L, Guo H Y, Xu G S, Liu S C, Gan K F, Wang H Q, Gong X Z, Liang Y, Zou X L, Hu J S, *et al.* 2014 *Nucl. Fusion* **54** 114002
[12] Liu X, Nielsen A H, Rasmussen J J, Naulin V, Olsen J, Xia T Y, Wang L, Deng G Z, Wu X Q, Liu Y, Wang Y M, Li Y Y, Zang Q, Xu G S and Li J 2019 *Phys. Plasmas* **26** 042509
[13] Chen M W, Yang X F, Gong X Z, Gan K F, Zhang B and Yang Z D 2020 *Fusion Eng. Des.* **150** 111415
[14] Meng L Y, Xu J C, Liu J B, Wang L, Qian X Y, Chen L, Liu X, Xu G S, Liang R R, Huang J, *el al.* 2021 *Nucl. Mater. Energy* **27** 100996
[15] Xu J C, Wang L, Xu G S, Luo G N, Yao D M, Li Q, Cao L, Chen L, Zhang W, Liu S C, *et al.* 2016 *Rev. Sci. Instrum.* **87** 083504
[16] Eich T, Leonard A W, Pitts R A, Fundamenski W, Goldston R J, Gray T K, Herrmann A, KirK A, Kallenbach A, Kardaun O, *et al.* 2013 *Nucl Fusion* **53** 093031
[17] Liu X, Naulin V, Xu J C, Deng G Z, Rasmussen J J, Liu J B, Nielsen A H, Goldston R J, Maingi R and Liu Y 2019 *Plasma Phys. Control. Fusion* **61** 045001
[18] Sieglin B, Eich T, Faitsch M, Herrmann A, Scarabosio A and the ASDEX Upgrade Team 2016 *Plasma Phys. Control. Fusion* **58** 055015